

LASER INTERFEROMETER GRAVITATIONAL WAVE OBSERVATORY
- LIGO -
CALIFORNIA INSTITUTE OF TECHNOLOGY
MASSACHUSETTS INSTITUTE OF TECHNOLOGY

Technical Note	LIGO-T1600153-v1	2016/11/01
Reference System for Cryogenic Coating Noise Measurements SURF Project 2016		
Subham Vidyant <i>Mentors : Dr. Johannes Eichholz, Dr. Christopher Wipf, Prof. Rana Adhikari</i>		

California Institute of Technology
LIGO Project, MS 18-34
Pasadena, CA 91125
Phone (626) 395-2129
Fax (626) 304-9834
E-mail: info@ligo.caltech.edu

Massachusetts Institute of Technology
LIGO Project, Room NW22-295
Cambridge, MA 02139
Phone (617) 253-4824
Fax (617) 253-7014
E-mail: info@ligo.mit.edu

LIGO Hanford Observatory
Route 10, Mile Marker 2
Richland, WA 99352
Phone (509) 372-8106
Fax (509) 372-8137
E-mail: info@ligo.caltech.edu

LIGO Livingston Observatory
19100 LIGO Lane
Livingston, LA 70754
Phone (225) 686-3100
Fax (225) 686-7189
E-mail: info@ligo.caltech.edu

Acknowledgement

This project would not have been possible if not for the constant guidance from my mentor Dr. Johannes Eichholz, who spent countless hours patiently mentoring me and explaining all the relevant concepts required to complete my work. I also thank my co-mentors Dr. Christopher Wipf and Prof. Rana Adhikari for their guidance and feedback. I would also like to thank Prof. Alan Weinstein for organizing all activities and engaging in a lot of productive discussions with us SURF students. Many thanks to Koji Arai, Gabriele Vajente, and Jess McIver for their valuable lectures. I would also like to thank Candace Rypisi and Carol Casey from the SFP office for always being there to help me.

I also thank Prof. Tarun Souradeep from IUCAA Pune, India and Prof. Anoop C S from IIT Kharagpur, India for their support.

Finally I would like to thank LIGO and Caltech for giving me an opportunity to spend 10 weeks here at Caltech and providing for the relevant financial and logistic aids.

Abstract

One source of noise the Advanced LIGO detectors and its proposed upgrades or any similar future detectors may struggle with is the Brownian noise in the coating of the mirrors, which can be reduced by using cryogenically cooled test masses. Its effect can be amplified by using short cavities. A workbench designed to measure the coating thermal noise in such cavities would benefit from an independent reference system with lower noise than the expected coating noise. A differential measurement of the test cavity resonance frequency fluctuations with that of the reference cavity would help us isolate the coating impact. This reference bench was setup after careful laser and cavity characterization and mode calculations. A visibility of 85% and a stable lock was achieved in the cavity and the output was guided back into the existing work bench to aid the characterization of coating noise.

Contents

1	Introduction	4
2	Coating Brownian Noise	4
3	Measurement of Coating Brownian Noise	5
3.1	Previous Experiment	5
3.2	Current Experiment	6
4	Methods	8
4.1	Gaussian Beams	8
4.2	Optical Cavities	9
4.3	Laser Mode Measurement	10
4.4	Mode Matching Tool	12
4.5	Pound-Drever-Hall Control Scheme	14
4.6	Laser Lock	16
4.7	Measurement of Cavity Pole : Glitch in Current Driver?	18
5	Results	19
A	Appendix	22
A.1	Matlab Code for Finding Beam Spot Size	22
A.2	Matlab Code for Finding Beam Waist	25

1 Introduction

The Laser Interferometer Gravitational-Wave Observatory (LIGO) is a large scale project aimed at detection and study of Gravitational Waves. The current Advanced LIGO Detectors are some of the most sophisticated and sensitive sensors for length fluctuations ever made. These interferometers measure strain in their arms in the order of 10^{-24} in the frequency range of 10 Hz to a few kHz. Instruments that aim at such delicate measurements are inherently prone to a wide range of noises. One such source of noise is the Brownian noise in the coating of the test masses.

In the present state of the LIGO detectors, the expected coating Brownian, or coating thermal noise level, is not yet observed. However, as commissioning goes on with the detector, the coating thermal noise will be as prominent as the quantum shot noise in the well of the sensitivity curve, as shown in Figure 1.

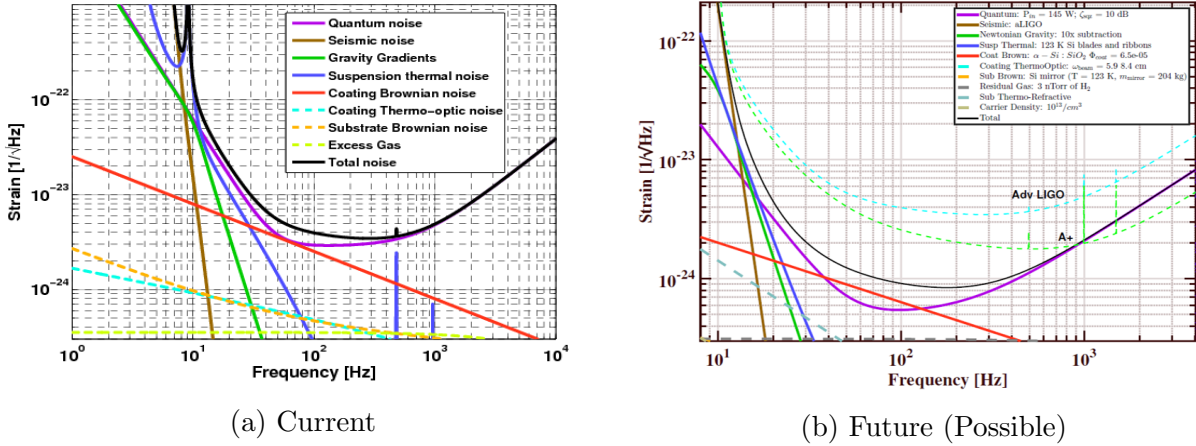


Figure 1: LIGO Noise Budget - On the left is the current LIGO noise budget. On the right is the predicted noise budget of the future LIGO detector after updates according to the 'Blue' design concept.[1]

Thus, any improvements in the reduction of quantum noise is useless unless accompanied by methods of reducing coating noise as well.

2 Coating Brownian Noise

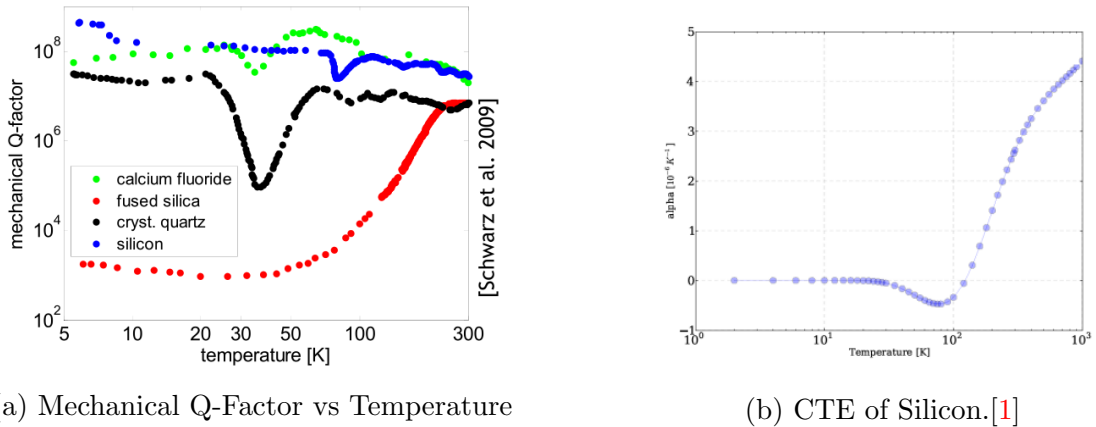
Coating Brownian noise arises from the coupling between macroscopic degrees of freedom and the thermal energy in the mirrors according to the fluctuation dissipation theorem[2]. To work out the thermal noise at a particular frequency f , one should mentally apply pressure oscillating at this frequency to the observed surface of the test mass[3]. The spatial profile of this pressure should mimic that of the light beam intensity. The power spectral density of thermal noise is then given by

$$S_x(f) = \frac{2k_B T W_{diss}}{\pi^2 f^2 F_0^2} \quad (1)$$

where k_B and T are Boltzmanns constant and the temperature of the mirror, respectively, F_0 deposits the amplitude of the oscillating force applied to the surface (i.e., the pressure integrated over the surface), and W_{diss} is the time-averaged power dissipated in the test mass when this oscillating pressure is applied. F_0 is an arbitrary amplitude needed for the calculation of W_{diss} , but cancels out in the final expression, since W_{diss} scales with F_0^2 .

While Brownian noise also emerges in the substrates and suspensions, the coating contribution presents a severe limitation to the achievable instrument performance between 40 and 200 Hz[4].

It is thus important to improve the mirror coatings and reduce the effects of this noise. A possible approach in doing so is cryogenically cooling the test masses so as to lower the thermal energy in the test mass, in turn lowering the Brownian noise. Due to the fact that the mechanical loss angle of fused silica increases towards lower temperatures, silicon is an attractive alternative for its mechanical properties and thermal characteristics[5], as shown in Figure 2. Moreover, silicon with its zero CTE at 123 K makes the whole interferometer very insusceptible to thermal problems, such as lensing. It is to be noted that KAGRA, the cryogenic GW detector currently under construction in Japan will use sapphire in the test mirrors.



(a) Mechanical Q-Factor vs Temperature

(b) CTE of Silicon.[1]

Figure 2: Mechanical And Thermal Properties Of Potential Substrate Materials.

3 Measurement of Coating Brownian Noise

3.1 Previous Experiment

A cryogenic test bench was constructed, whose optical setup is schematically shown in Figure 3, and was designed to measure coating noise in test mirrors. The bench consisted of two nominally identical optical cavities inside a liquid nitrogen cryostat with independent lasers

locked to them. The cavities were made with test mirrors using silicon as the substrate with tantala-silica coatings. Using this setup for a differential measurement of the resonance frequency fluctuations in the two cavities, a direct measure of coating thermal noise that dominates these cavities by design can be obtained.

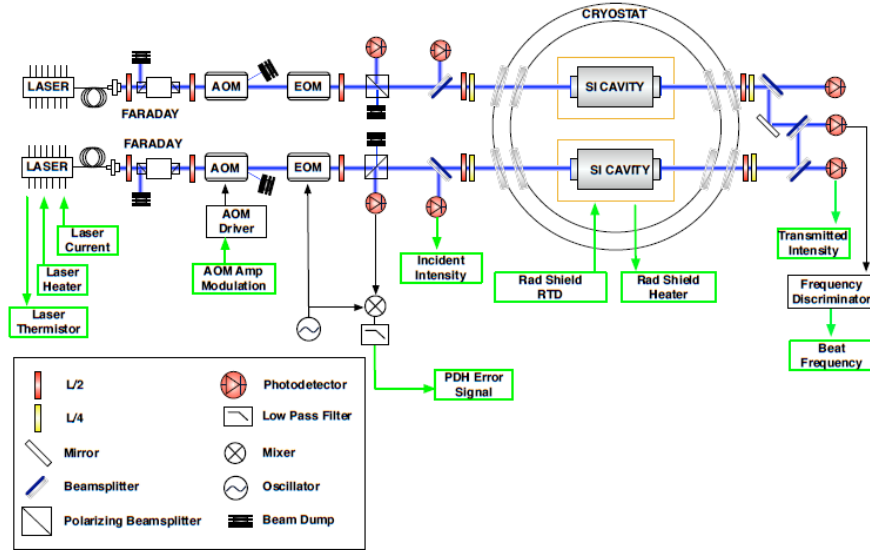


Figure 3: Old Setup.

Unlike LIGO in its current state, the experiment used silicon optics because fused silica is not well-suited as a substrate material at cryogenic temperatures due to increased mechanical loss and low thermal conductivity. This in turn required a transition to 1550 nm lasers, because silicon is too absorptive at 1064 nm. To take full advantage of its superior properties, both spacer and mirrors were made from silicon.

However the results showed that the coating noise was overshadowed by the other undesirable noises from various sources and was not observed. Thus a more sensitive setup was required.

3.2 Current Experiment

A few changes were made to the setup to make the experiment more sensitive. Better current drivers with increased bandwidth were used. The old test cavities will be replaced with new shorter ones. The free spectral range, or FSR, of a cavity is related to its length L by

$$FSR = \frac{c}{2L} \quad (2)$$

These next generation test cavities are 3.7 cm long, and thus have a large free spectral range of 4.05 GHz. They enhance the conversion from length fluctuations due to coating thermal noise to frequency fluctuations.

However due to manufacturing tolerances in the length of these cavities, the relative location of the resonances are somewhat uncertain, and a small difference in their lengths can result

in the locking frequencies to be far apart. Thus it is very likely that beat frequency will be too high to be detectable by the photo detector used in the experiment.

Thus as a contingency plan for these beat measurements and a diagnostic tool for debugging the original test bench, the proposed modification of the setup is the addition of an external reference system, as shown in Figure 4.

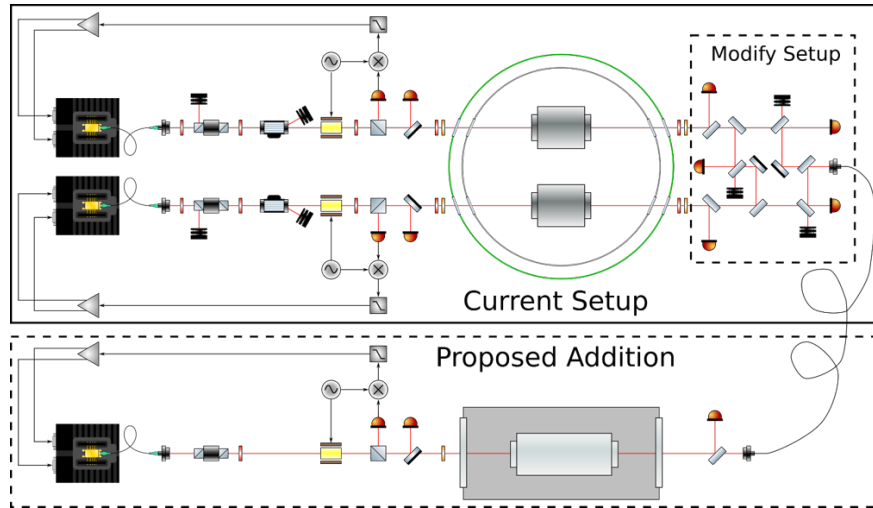


Figure 4: New Setup with the added Reference Cavity.

The cavity to be used in this reference system, shown in Figure 5, is much longer than the next generation test cavities (8 inches) and supports larger beams, which dilutes the impact of coating noise. The large length implies that it has a small free spectral range of 738.2 MHz. Thus even if the locking frequencies of the two test cavities are far apart, when they are compared with the reference cavity individually, it is possible to find pairs of resonances no further apart than half its FSR. The reference cavity is therefore intrinsically less prone to coating thermal noise and will be used as a frequency reference for the coating noise induced frequency fluctuations in the test cavities. Similar cavities have been used in the past for room temperature measurements of coating thermal noise[6].

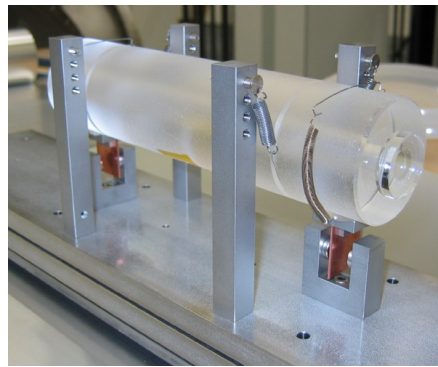


Figure 5: Reference Cavity - While identical in shape, the cavity used for the presented project was missing the eddy-current damping displayed here.

The lasers used in the experiment are fibre coupled diode lasers. They operate around the required wavelength of 1550 nm.

4 Methods

4.1 Gaussian Beams

A Gaussian beam is a beam of monochromatic electromagnetic radiation whose transverse magnetic and electric field amplitude profiles are given by the Gaussian function, as shown in Figure 6.

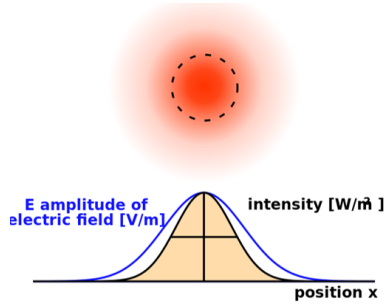


Figure 6: Intensity Profile of a Gaussian Beam.

The mathematical expression for the electric field amplitude is a solution to the paraxial Helmholtz equation. Assuming polarization in the x direction and propagation in the $+z$ direction, the electric field in phasor (complex) notation is given by

$$\mathbf{E}(r, z) = E_0 \hat{x} \frac{w_0}{w(z)} \exp\left(\frac{-r^2}{w(z)^2}\right) \exp\left(-i\left(kz + k\frac{r^2}{2R(z)} - \psi(z)\right)\right) \quad (3)$$

Any Gaussian beam of a given wavelength λ can be fully described by two properties, namely its waist w_0 , which is its radius at its narrowest location, and the location z_0 of this waist[7]. At a position z along the beam, the spot size parameter w is given by

$$w(z) = w_0 \sqrt{1 + \left(\frac{z - z_0}{z_R}\right)^2} \quad (4)$$

which is qualitatively plotted in Figure 7.

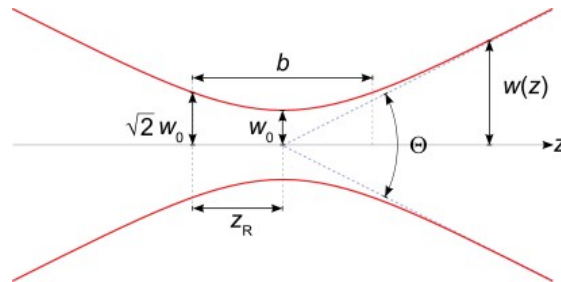


Figure 7: Beam Profile of a Gaussian Beam.

The wavefront of a Gaussian beam is flat at the beam waist and is asymptotically flat at $z \rightarrow \pm\infty$. $R(z)$ is the radius of curvature of the wavefront as a function of position along the beam, given by

$$R(z) = z \left[1 + \left(\frac{z_R}{z - z_0} \right)^2 \right] \quad (5)$$

where z_R is called the Rayleigh range and is given by

$$z_R = \frac{\pi w_0^2}{\lambda} \quad (6)$$

At a distance from the waist equal to the Rayleigh range z_R , the width w of the beam is $\sqrt{2}$ larger than it is at the focus.

4.2 Optical Cavities

An optical cavity is an arrangement of mirrors that forms a closed optical path resonator for light waves. The most commonly used laser resonators are composed of two spherical mirrors facing each other[7]. Light confined in the cavity produce standing waves for certain resonance frequencies due to multiple reflections from the mirrors. Only certain patterns and frequencies of radiation will be sustained by the resonator, with the others being suppressed by destructive interference. In general, radiation patterns which are reproduced on every round-trip of the light through the resonator are stable, and these are the eigenmodes, known as the modes, of the resonator. The geometries of the cavity mirrors determine the mode which will resonate in the cavity. Figure 8 shows the modes resonant in different types of cavities.

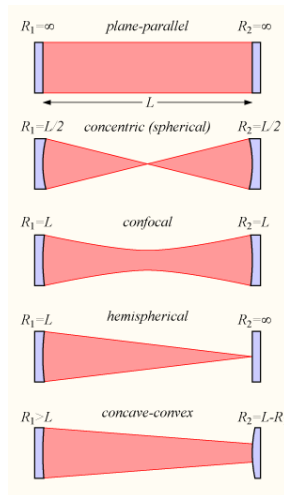


Figure 8: Effect of Cavity Geometry on Resonant Mode.

When a mode resonates, its wavefronts are coincident with the mirror surface. In a simple Fabry-Perot cavity only spatial modes whose wavefronts match the curvature of the mirror surfaces upon reflection can resonate. However, with multi-mirror cavities, that are present in the LIGO detectors, this is not necessarily true anymore, as requirement for resonance is that the laser mode is eventually projected into itself. This principle of wavefronts coinciding with mirror surfaces is used to find the resonant mode in the mode matching calculations.

The reference cavity is 8 inches or 20.32 cm long and has one flat mirror, and one concave mirror with a radius of curvature (ROC) of 50 cm. Using Equations (5) and (6), the waist of the resonant beam was obtained to be 348.2 μm and located at the surface of the plane mirror.

The intensity transmitted by a cavity is a function of the frequency of light, if the mode and cavity dimensions remain unchanged. The finesse of an optical cavity is defined as its free spectral range divided by the FWHM (full width at half-maximum) bandwidth of its resonances[8].

$$\mathcal{F} = \frac{\text{FSR}}{\text{FWHM}} \quad (7)$$

The plot of two cavities with different finesse is shown in Figure 9.

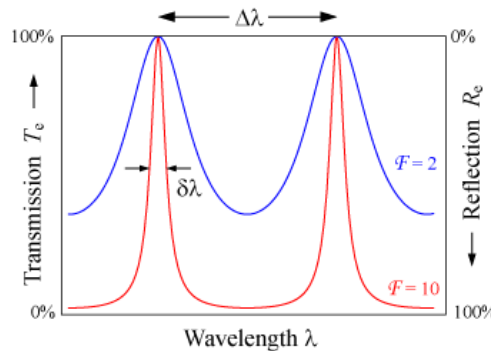


Figure 9: Intensity Curve of an Optical Cavity.

The peaks correspond to the resonant frequencies. Cavities with higher finesse have sharper peaks at the resonance frequencies.

4.3 Laser Mode Measurement

The differential measurement of the cavity outputs is made in transmission, therefore it is necessary to get as much light through as possible. This dictates that the laser mode entering the cavity must be close to the cavity resonant mode. This transformation is usually accomplished with a collection of thin lenses[7]. However, one must have prior knowledge of the existing beam profile exiting the collimator before attempting to find the lens solution.

The electric field vector of the laser is given by Equation (3). The second exponent is purely imaginary and denotes the phase of the electric field. Hence it can be neglected

while calculating the power of the laser. The radial coordinate system is changed into the Cartesian coordinate system. If a vertical barrier is placed from the abscissa negative infinity to x , the power transmitted past this barrier is

$$P(x) = \int_{-\infty}^{+\infty} \int_x^{+\infty} E_0^2 \frac{w_0^2}{w(z)^2} e^{-\frac{2(x'^2+y^2)}{w(z)^2}} dx' dy \quad (8)$$

$$= \frac{E_0^2 w_0^2 \pi}{8} \left[1 - \operatorname{erf} \left(\frac{2x}{w(z)} \right) \right] \quad (9)$$

Therefore, the coefficient of x in the above function is half of the inverse of the beam spot size at that point.

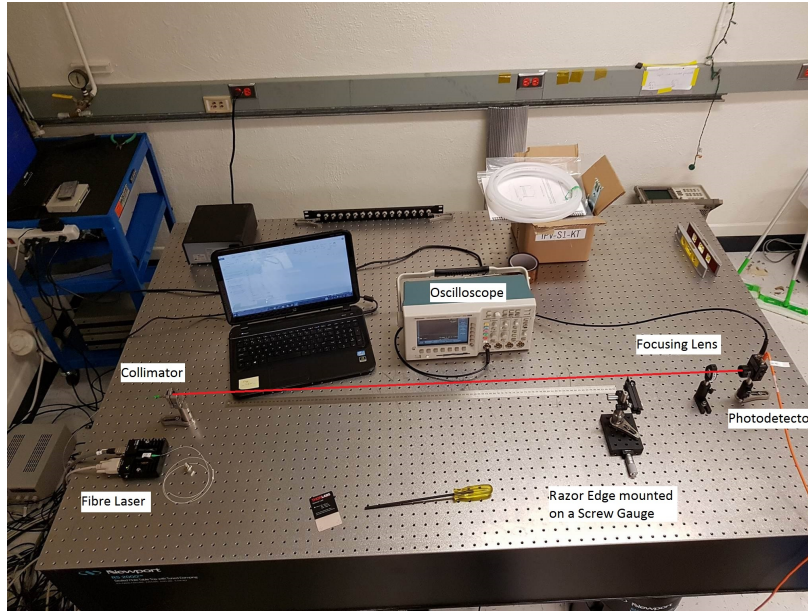


Figure 10: Setup For Finding Beam Parameters.

A razor blade was used to obstruct the beam at various depths. A photodetector measured the power transmitted after the obstruction and the characteristic curve was obtained by plotting the edge depth vs power transmitted, as shown in Figure 11. The razor edge eclipses the beam at different distances, allowing only a part of the beam to propagate, resulting in the observed integrated intensity curve. This curve is characteristic of the beam spot size at that location, as shown in Equation (9). This curve was then fitted to an error function (code in Appendix A.1) and the fitting parameter corresponding to the coefficient of x gave the beam spot size at that point. This was repeated at various distances from the laser collimator and the beam spot size was found at every such point and plotted, as shown in Figure 12. Fitting this curve to a beam profile (given in Equation (4)) using a least square fitting algorithm (code in Appendix A.2) and extending the plot gave us the beam waist and its location from the collimator. This complete procedure was repeated after turning the collimator by 90° . All fitting operations were done using Matlab.

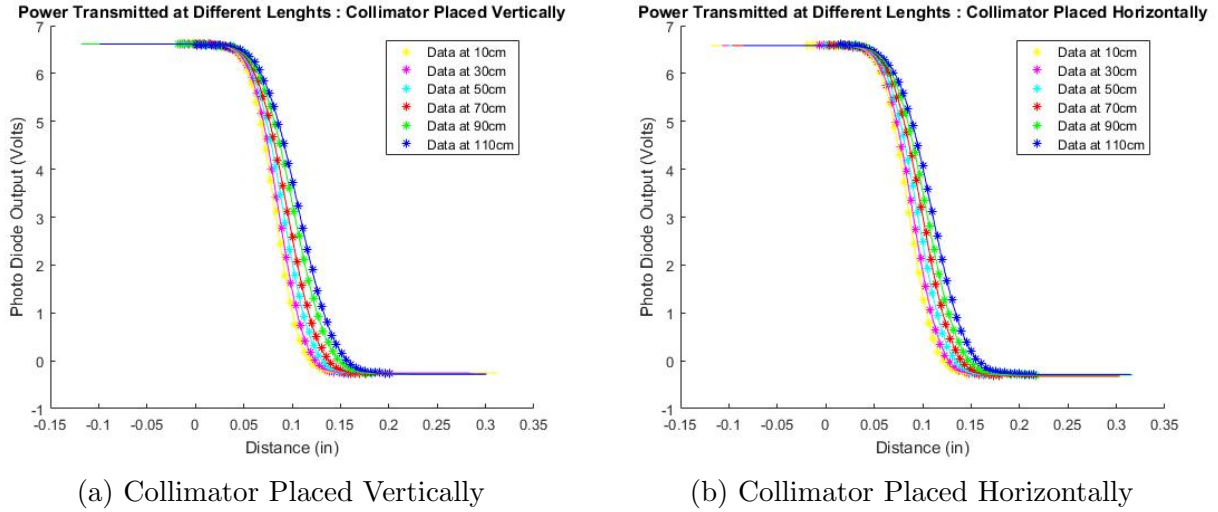


Figure 11: Photo-Diode Output at Various Distances From Collimator

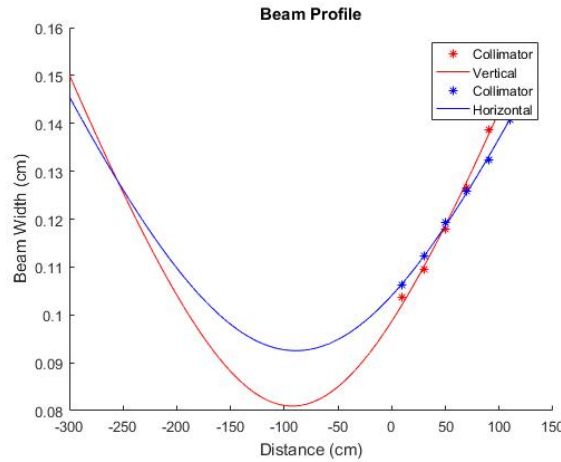


Figure 12: Beam Spot-Size Along Beam Axis.

The beam waist (with the collimator placed vertically) was found out to be $810 \mu\text{m}$ at a distance of 92.53 cm behind the collimator, making it a virtual waist on the fiber side. The beam waist (with the collimator placed horizontally) was found out to be $925 \mu\text{m}$ at a distance of 89.23 cm behind the collimator. The average of the two was used to approximate the beam waist and location for the mode matching calculations.

4.4 Mode Matching Tool

After the initial laser mode and the laser mode supported by the cavity was determined, a mode matching software (Just Another Mode Matching Tool or JamMt) was used to find a lens solution which changes the initial mode to the required mode.

Some components like the Electro-Optic Modulator (EOM) have beam spot size restrictions. The one used in this setup has an aperture of 2 mm . These restrictions are considered, so are the distances of the components and cavity from the collimator. A suitable lens solution

which is easy to set up and provides the required laser mode to a certain tolerance was obtained by placing the EOM at a distance of 65 cm from the collimator. At this distance, using a 400 mm convex lens placed at a distance of 20 cm, the waist of the beam was 206.308 μm and was positioned at around 64 cm, close enough to the EOM and small enough that the beam passes freely through the EOM without obstruction, as shown in Figure 13.

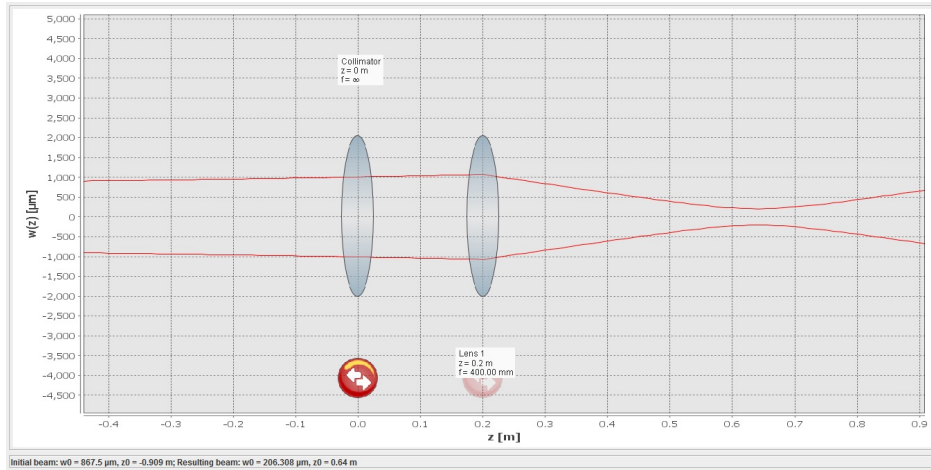


Figure 13: Screen-shot from the mode matching software (beam path up to the EOM).

Then, after considering the dimensions of the vacuum tank and the optical table, a crude estimate of the position of the reference cavity was determined to be around 270 to 300 cm. Thus a beam waist of 348.2 μm was needed at about 270 cm from the collimator. This was achieved within the tolerance limit by placing 3 convex lenses of focal lengths 200 mm, 225 mm, and 250 mm at positions 85 cm, 160 cm and 224 cm in front of the collimator respectively, as shown in Figure 14. This setup gave a theoretical beam waist of 352.979 μm at a distance of 285 cm. After some fine adjustments and lens repositioning, the laser mode finally obtained had a waist of around 353 μm at 285 cm.

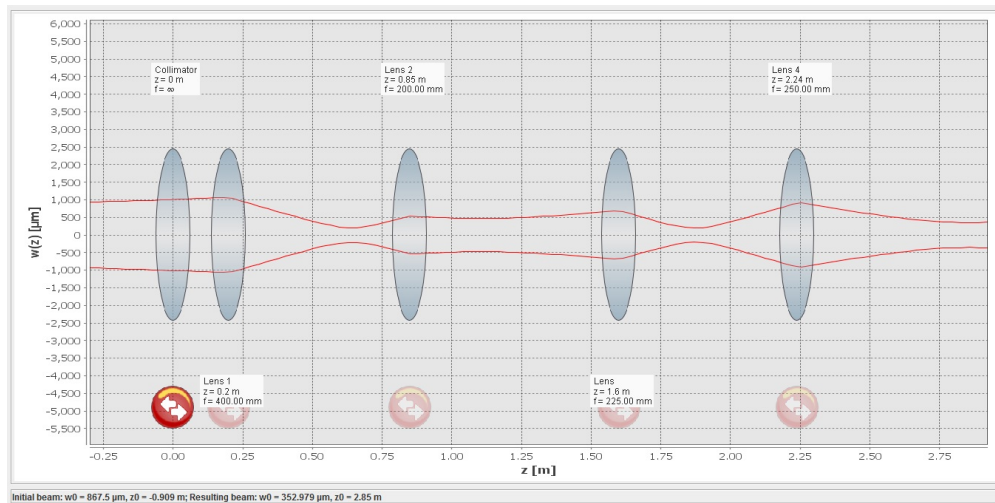
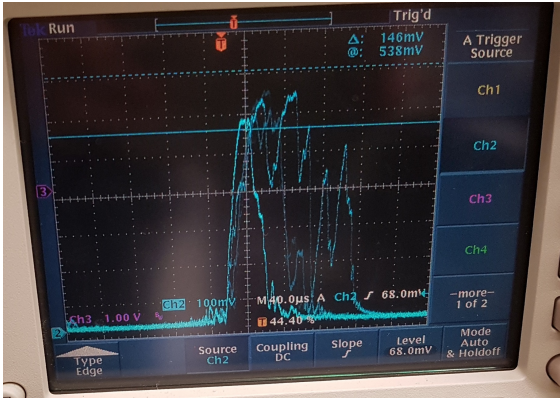


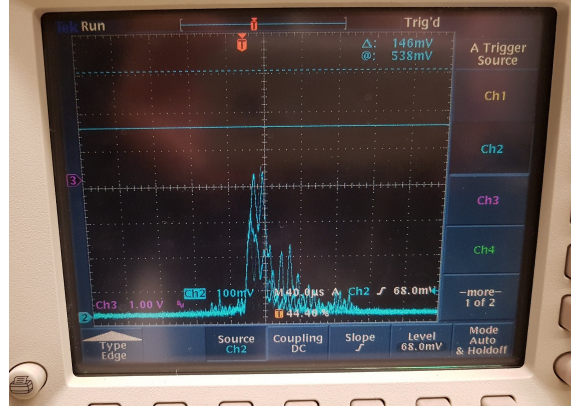
Figure 14: Lens positions for Mode Matching.

The cavity was placed according to the position calculated and the laser frequency was scanned using a ramp modulation of the laser injection current (which is the primary frequency tuning mechanism for the used lasers) across a range of $2 V_{p-p}$ to observe the transmitted 00 mode using a CCD camera and a photodiode. A Faraday isolator, which is an optical diode, was added to the setup to help reduce the laser noise. If the mode matching is done perfectly, the light reflected back by the cavity will retrace its path and enter the collimator. This light, or any other spurious back-reflections and scattered light on the way there, will enter the laser cavity and destabilize the laser adding frequency noise. The addition of a diode gets rid of this reflected light and keeps the laser stable. After optimizing the beam alignment, a transmission through the cavity was obtained, the photodetector signal of which is shown in Figure 15. The visibility of the setup, which is the fraction of the incident light that resonates in the fundamental mode (Equation (10)), was then determined by manually scanning the laser over one free spectral range and noting the power transmitted for different modes transmitted by the cavity. Adding all the transmitted powers and dividing by the total power of the laser, the visibility was found to be 85%.

$$\text{Visibility} = \frac{\text{Intensity resonating in cavity}}{\text{Total incident intensity}} = \frac{\text{Power transmitted for required mode}}{\text{Power transmitted for all modes}} \quad (10)$$



(a) Before adding faraday isolator



(b) After adding faraday isolator

Figure 15: Photodiode output of transmitted 00 mode : The output before had a lot of noise beyond the peak. Upon addition of the Faraday Isolator, we see a reduction of the noise and the peak is much more prominent.

4.5 Pound-Drever-Hall Control Scheme

Once the laser mode is the same as the resonant mode of the cavity, all, or a majority of the light, depending on the visibility, is transmitted through, and the light can resonate in the cavity if it maintains the right frequency. However, this state does not remain as such as both the laser frequency and cavity length drift away. As the cavity used is of high finesse, any fluctuations in the frequency of the laser or the dimensions of the cavity will throw the laser off resonance. Thus there is a need for a feedback system which constantly detects any

changes to the system and changes the laser frequency to maintain a resonant condition. This state where the resonance is forcefully held without interruption is called lock.

The Pound-Drever-Hall[9] scheme, which is illustrated in Figure 16, is such a system. The beam enters the cavity while a photodetector is used, along with a halfwave plate and polarizing beam-splitter, to detect the reflected beam. The output goes to an actuator that controls the frequency of the laser. When the loop is closed, the system will automatically adjust the frequency until the light is resonant and then hold it there. The feedback circuit compensates for any disturbance (within reason) that tries to bump the system out of resonance. A record of how much force the feedback circuit supplies gives a measurement of the noise in the cavity.

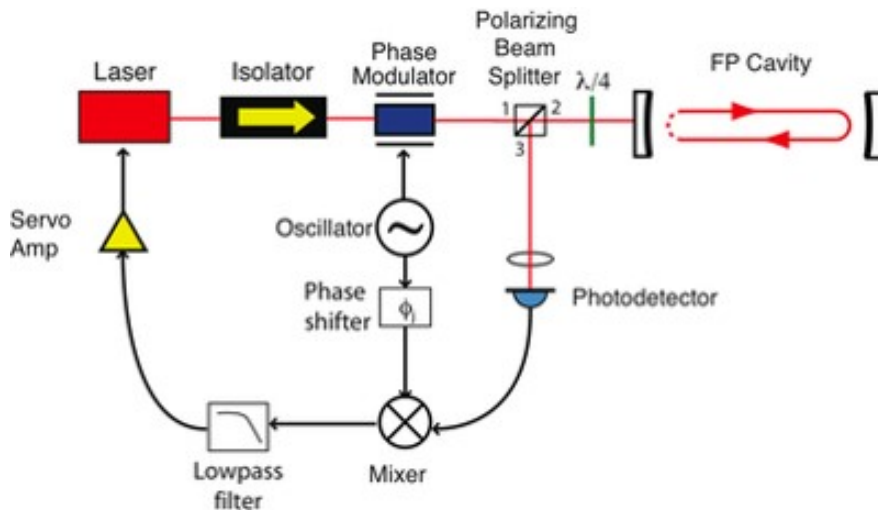


Figure 16: Pound-Drever-Hall Schematic.

In Figure 16, the Phase modulator modulates the phase of the laser beam, and the reflected light is compared with the modulation signal from the oscillator. The phase modulator imprints sidebands on the carrier $w_0 - w_m$ and $w_0 + w_m$, where w_0 is the carrier frequency and w_m is the modulation frequency. These sidebands are far from the cavity resonance frequency. Due to the nature of phase modulation, one sideband is in phase and one is out of phase with respect to the carrier. Near resonance, the carrier experiences a phase shift that the sidebands are not affected by. By demodulating the correct quadrature of the back-reflected light against the modulation signal, one obtains an error signal with the desired properties.

The mixer compares the modulation signal (generated by the oscillator in Figure 16) with the output of the photodetector, extracting the part that is at the same frequency as the modulation signal. (The mixer's output is just the product of its inputs.) The sign of the mixer's lowpass filtered output is different on either side of resonance, and it is zero when the system is exactly on resonance (if the correct quadrature is demodulated), as shown in Figure 17. Thus this signal can be used as a feedback control signal. In control theory, this feedback signal is called the error signal. Sending this error signal after passing through a PI Controller/Servo Amplifier to the laser current driver's modulation input completes the feedback loop and locks the system on resonance.

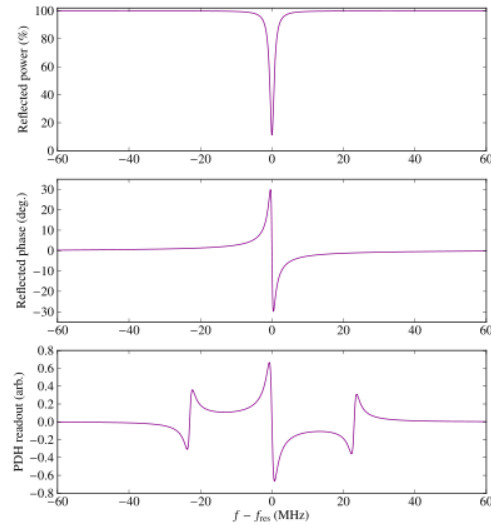


Figure 17: PDH Error Signal - Depicting the Reflected Power %, Reflected Phase and PDH Readout vs the frequency error.

4.6 Laser Lock

A typical choice for a PDH setup is a modulation index of 0.3. As per the datasheet of the EOM, the half wave voltage for light of wavelength 1550 nm was around 330 V. Thus to get a modulation of 0.3 radians, a signal of 34 dBm was needed. The mixer used was of level 7 (7 dBm), therefore a 10 dBm signal was generated and split. The other 7 dBm signal was too large for the low noise amplifier of 36 dB used. So a 16 dB attenuator was added to avoid overdriving the amplifier. Finally a resonant circuit of 6 dB was added to reach the desired voltage. The light was modulated at the resonant frequency and the sidebands were observed on the photodiode by sweeping the laser with a ramp signal. With these modulated sidebands, the tuning coefficient of the laser was determined to be 11.32 MHz/V. A delay line (which is essentially a long cable to delay the phase) for the feedback loop was added to correct for the phase difference in the two paths and set the correct demodulation phase. A better error signal, which is shown in Figure 18, was obtained by varying the cable length and making some fine adjustments to the modulating frequency.

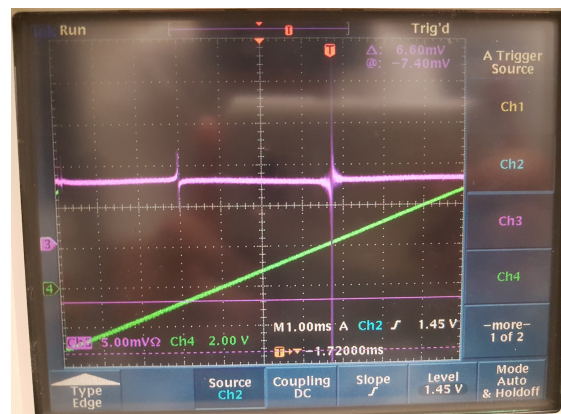


Figure 18: Error signal depicting carrier band and one side band.

The cavity pole is related to the FSR and finesse \mathcal{F} of a cavity according to the equation

$$\text{CavityPole} = \frac{\text{FSR}}{2\mathcal{F}} \quad (11)$$

The free spectral range of the cavity was known to be 738.2 MHz and the cavity was known to be of high finesse (≈ 5000), using which the pole location of the cavity was estimated to be around 70kHz and the PI controller was set as a pure integrator (as the pole would be far from the operating range of the feedback system) with 30 dB low frequency cutoff and a gain of around 5. Then by slowly changing the servo amp output offset, a solid lock of the 00 mode was achieved. The transmitted 00 mode is shown in Figure 19.

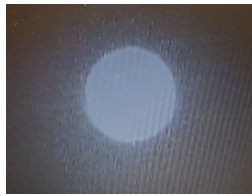


Figure 19: Beam spot as seen on the CCD camera

The dynamic range of the current frequency feedback was too small and hence the laser was unable to remain locked to the cavity for extended periods of time, due to the slow change in the ambient temperature causing the length of the cavity to gradually change. A possible solution to this would be to use a second hierarchical feedback loop for the laser temperature which has a much larger frequency response, but at a much reduced bandwidth of only several Hz. This way the current control will take care of the faster actuations much more effectively and remain in its operating range. For the stability of the laser it was found to be important to be in the upper branch of the laser power vs injection current setting hysteresis curve shown in Figure 20. Note that this characteristic depends on the temperature operating point.

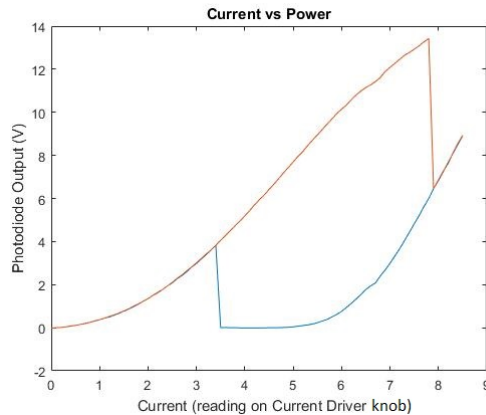
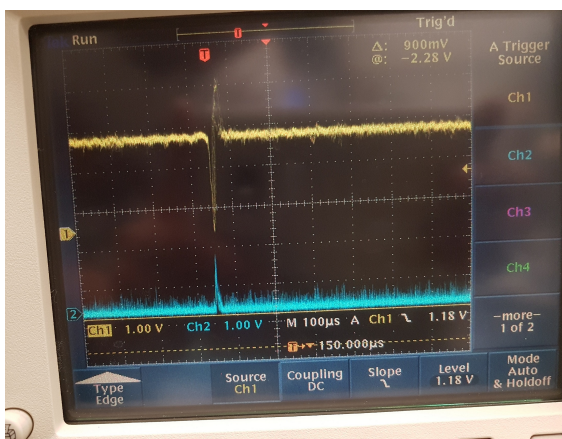


Figure 20: Current VS Power hysteresis of the laser : This hysteresis behavior is a result of a transition between competing longitudinal modes.

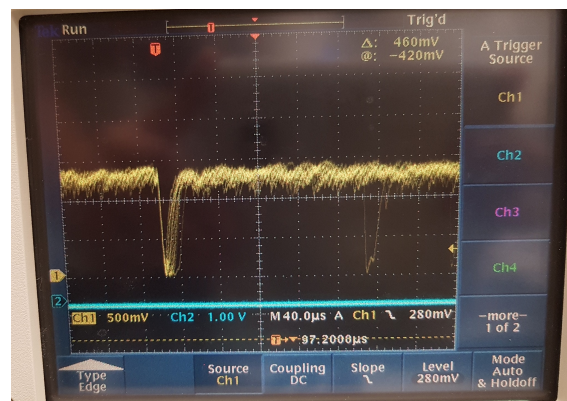
4.7 Measurement of Cavity Pole : Glitch in Current Driver?

By measuring the cavity pole, a better feedback loop for the cavity can be designed. To conduct this measurement, an AOM (Acousto-Optic Modulator) was added to the reference bench to modulate the light amplitude, because it has the same response in the cavity as a frequency modulation. The AOM was placed immediately after the EOM (where the beam spot size was relatively small) and the deflected light was blocked off by a beam dump. The modulating chirp signal from the network analyzer was used to drive the AOM driver. This way, the transmitted light intensity transfer function for the setup could be found. A direct measurement of the cavity transfer function would be polluted by the transfer functions of various electronic components. Hence, by doing the measurement twice, once with the cavity in place and then with it removed, the transfer functions with and without the cavity would be obtained. Then by dividing these two, one would get the frequency response of the cavity, and finally the cavity pole from its -3 dB cutoff point.

However, despite well-in-range signal levels, the network analyzer was indicating an overload on the transmitted light input. Upon looking at the transmitted light intensity from the photodetector on an oscilloscope, it seemed that the signal had an occasional glitch which was the likely cause of the overload. The glitch had no clear periodicity but had a distinct shape, which indicates excess low frequency noise of the laser that an optimized feedback controller needs to take into account. It was unaffected by the gain of the servo amplifier which might indicate that it originated in the current driver or the laser. Moreover, changing the driving current of the laser seemed to change the shape of the glitch. At a higher driving current, the glitch had an overshoot, but at a lower driving current, the overshoot was absent and the shape looked as if it was damped, as shown in Figure 21, which seems to indicate that the noise properties of the laser change with the injection current bias.



(a) With laser at a higher operating point



(b) With laser at a lower operating point

Figure 21: Glitch observed in transmitted light

5 Results

The vacuum tank was placed and the cavity was put inside it. The alignments were re-adjusted and the feedback parameters were fine tuned. The servo amplifier was set as a pure integrator with the corner frequency fixed at 30 dB and the gain set to 5. Then the transmitted light was split by a 90:10 beam-splitter and the majority of the light was coupled back into a fiber (as shown in Figure 4), to be transferred to the test bench, after the required mode matching calculations, as shown in Figure 22.

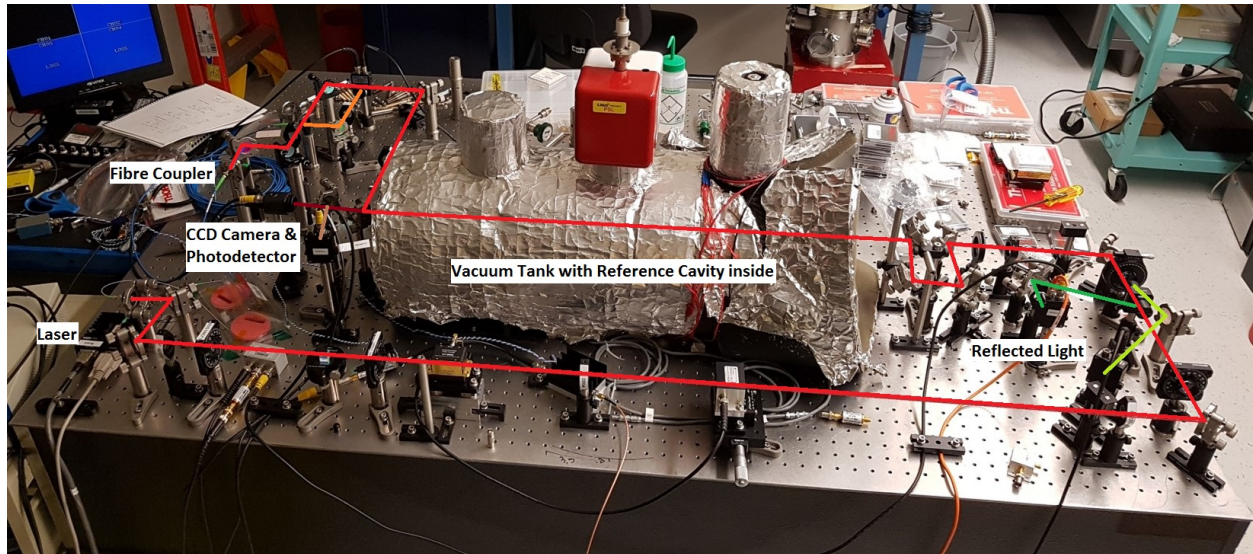


Figure 22: Final Setup.

With the laser finally locked on to the cavity, the feedback loop transfer function was measured using a network analyzer and is shown in Figure 23

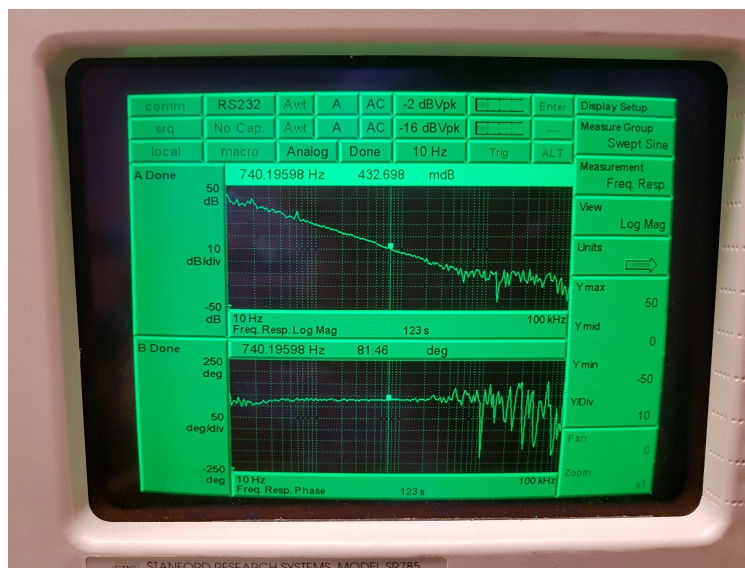


Figure 23: Transfer Function and Phase : The magnitude plot has a slope of -20 dB/dec up to about 10 kHz after which it flattens out. The phase appears to be flat until about 10 kHz.

The loop was characterized and the Cavity Transfer Function and Closed Loop Transfer Function of Open Loop Gain were found. They are as follows

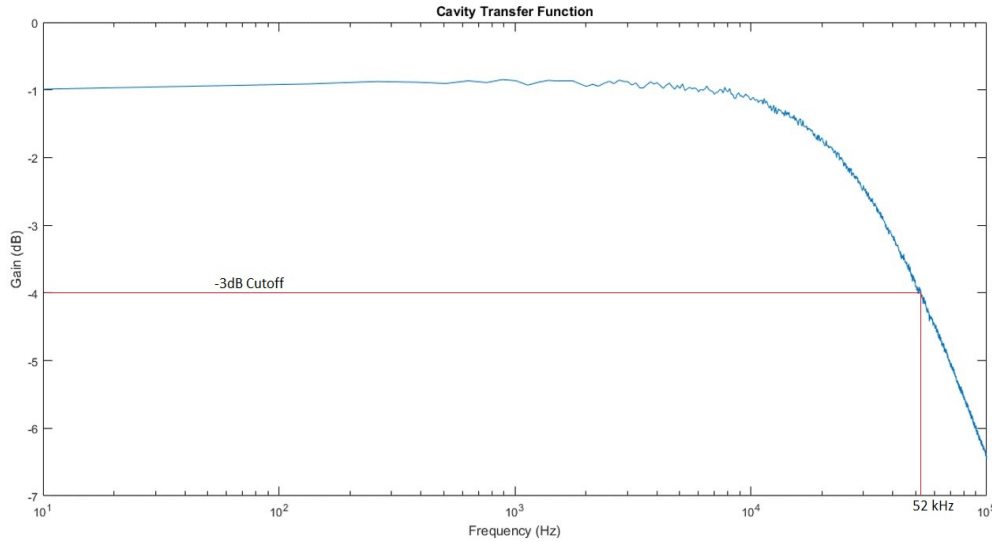


Figure 24: Cavity Transfer Function : The -3 dB cutoff is at 52 kHz, which represents the cavity pole. Hence the linewidth of the cavity is 104 kHz.

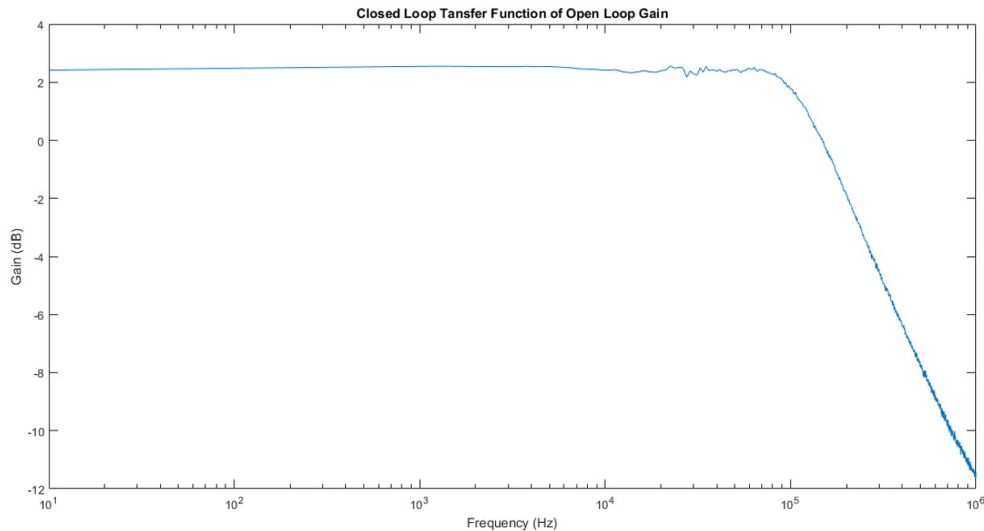


Figure 25: Closed Loop Transfer Function - The gain is flat at a little above 2 for low frequencies, while it should be at 0. This is due to an impedance imbalance in the input ports of the network analyzer.

The intensity of light exiting the fiber was found to be 1.8 mW. Hence the Fibre Coupling Efficiency was calculated to be 26%. A proper characterization of the desired fiber input mode and better effort with mode matching could increase this efficiency further. The cavity pole was observed to be at 52 kHz and the Finesse of the cavity was found to be 7100 (using Equation (11)). The visibility was 85%.

References

- [1] e. a. Rana Adhikari, “LIGO Voyager Upgrade Conceptual Design,” p. 8 (2016). LIGO-T1400226-v7.
- [2] Y. Levin, “Internal thermal noise in the LIGO test masses: A direct approach,” *Phys. Rev. D* **57**, 659–663 (1998).
- [3] Y. Levin, “Fluctuation - dissipation theorem for thermo-refractive noise,” *Phys. Lett. A* **372**, 1941–1944 (2008).
- [4] T. Hong, H. Yang, E. K. Gustafson, R. X. Adhikari, and Y. Chen, “Brownian thermal noise in multilayer coated mirrors,” *Phys. Rev. D* **87**, 082001 (2013).
- [5] J. Franc, N. Morgado, R. Flaminio, R. Nawrodt, I. Martin, L. Cunningham, A. Cumming, S. Rowan, and J. Hough, “Mirror thermal noise in laser interferometer gravitational wave detectors operating at room and cryogenic temperature,” arXiv (2009). <http://arxiv.org/abs/1506.07088>.
- [6] T. Chalermongsak, F. Seifert, E. D. Hall, K. Arai, E. K. Gustafson, and R. X. Adhikari, “Broadband measurement of coating thermal noise in rigid Fabry-Pèrot cavities,” *Metrologia* **52**, 17 (2015).
- [7] H. Kogelnik and T. Li, “Laser beams and resonators,” *Appl. Opt.* **5**, 1550–1567 (1966).
- [8] A. E. Siegman, “Lasers,” p. 435.
- [9] E. D. Black, “An introduction to Pound-Drever-Hall laser frequency stabilization,” *American Journal of Physics* **69**, 79–87 (2001).

A Appendix

A.1 Matlab Code for Finding Beam Spot Size

```

1 filename = 'H_10 cm.dat';
2 delimiterIn = '';
3 A1 = importdata(filename, delimiterIn);
4 z1 = A1(:,1);
5 w1 = A1(:,2);
6 F1 = @(x1, z1) ((x1(1)*erf((x1(2)*z1)-x1(3)))+x1(4));
7 x10 = [7 3 0 0];
8 [x1, resnorm, ~, exitflag, output] = lsqcurvefit(F1, x10, z1, w1);
9
10 filename = 'H_30 cm.dat';
11 delimiterIn = '';
12 A2 = importdata(filename, delimiterIn);
13 z2 = A2(:,1);
14 w2 = A2(:,2);
15 F2 = @(x2, z2) ((x2(1)*erf((x2(2)*z2)-x2(3)))+x2(4));
16 x20 = [7 3 0 0];
17 [x2, resnorm, ~, exitflag, output] = lsqcurvefit(F2, x20, z2, w2);
18
19 filename = 'H_50 cm.dat';
20 delimiterIn = '';
21 A3 = importdata(filename, delimiterIn);
22 z3 = A3(:,1);
23 w3 = A3(:,2);
24 F3 = @(x3, z3) ((x3(1)*erf((x3(2)*z3)-x3(3)))+x3(4));
25 x30 = [7 3 0 0];
26 [x3, resnorm, ~, exitflag, output] = lsqcurvefit(F3, x30, z3, w3);
27
28 filename = 'H_70 cm.dat';
29 delimiterIn = '';
30 A4 = importdata(filename, delimiterIn);
31 z4 = A4(:,1);
32 w4 = A4(:,2);
33 F4 = @(x4, z4) ((x4(1)*erf((x4(2)*z4)-x4(3)))+x4(4));
34 x40 = [7 3 0 0];
35 [x4, resnorm, ~, exitflag, output] = lsqcurvefit(F4, x40, z4, w4);
36
37 filename = 'H_90 cm.dat';
38 delimiterIn = '';
39 A5 = importdata(filename, delimiterIn);
40 z5 = A5(:,1);
41 w5 = A5(:,2);
42 F5 = @(x5, z5) ((x5(1)*erf((x5(2)*z5)-x5(3)))+x5(4));
43 x50 = [7 3 0 0];

```

```

44 [x5, resnorm, ~, exitflag, output] = lsqcurvefit(F5, x50, z5, w5);
45
46 filename = 'H_110 cm.dat';
47 delimiterIn = '';
48 A6 = importdata(filename, delimiterIn);
49 z6 = A6(:, 1);
50 w6 = A6(:, 2);
51 F6 = @(x6, z6)((x6(1)*erf((x6(2)*z6)-x6(3)))+x6(4));
52 x60 = [7 3 0 0];
53 [x6, resnorm, ~, exitflag, output] = lsqcurvefit(F6, x60, z6, w6);
54
55 hold on;
56 b = (-1:0.001:3);
57 a1 = ((x1(1)*erf((x1(2)*b)-x1(3)))+x1(4));
58 a2 = ((x2(1)*erf((x2(2)*b)-x2(3)))+x2(4));
59 a3 = ((x3(1)*erf((x3(2)*b)-x3(3)))+x3(4));
60 a4 = ((x4(1)*erf((x4(2)*b)-x4(3)))+x4(4));
61 a5 = ((x5(1)*erf((x5(2)*b)-x5(3)))+x5(4));
62 a6 = ((x6(1)*erf((x6(2)*b)-x6(3)))+x6(4));
63
64 err5 = max(a6)-max(a5);
65 err4 = max(a6)-max(a4);
66 err3 = max(a6)-max(a3);
67 err2 = max(a6)-max(a2);
68 err1 = max(a6)-max(a1);
69
70 e1 = z3(18)-z1(18) -0.19;
71 e2 = z3(18)-z2(18) -0.07;
72 e4 = z3(18)-z4(18) +0.035;
73 e5 = z3(18)-z5(20) +0.27;
74 e6 = z3(18)-z6(20) +0.25;
75
76 plot((z1+e1)/10, w1+err1, 'y*');
77 plot((z2+e2)/10, w2+err2, 'm*');
78 plot(z3/10, w3+err3, 'c*');
79 plot((z4+e4)/10, w4+err4, 'r*');
80 plot((z5+e5)/10, w5+err5, 'g*');
81 plot((z6+e6)/10, w6, 'b*');
82
83 plot((b+e1)/10, a1+err1, 'y');
84 plot((b+e2)/10, a2+err2, 'm');
85 plot(b/10, a3+err3, 'c');
86 plot((b+e4)/10, a4+err4, 'r');
87 plot((b+e5)/10, a5+err5, 'g');
88 plot((b+e6)/10, a6, 'b');
89

```

```
90 title('Power Transmitted at Different Lengths : Collimator Placed  
    Horizontally');  
91 xlabel('Distance (in)');  
92 ylabel('Photo Diode Output (Volts)');  
93 legend('Data at 10cm', 'Data at 30cm', 'Data at 50cm', 'Data at 70cm',  
    , 'Data at 90cm', 'Data at 110cm');  
94 hold off;
```

A.2 Matlab Code for Finding Beam Waist

```

1 filename = 'V_Waist.dat';
2 delimiterIn = ' ';
3 A1 = importdata(filename, delimiterIn);
4 z1 = A1(:,1);
5 w1 = A1(:,2);
6 w1 = w1*0.254;
7
8 filename = 'H_Waist.dat';
9 delimiterIn = ' ';
10 A2 = importdata(filename, delimiterIn);
11 z2 = A2(:,1);
12 w2 = A2(:,2);
13 w2 = w2*0.254;
14
15 hold on;
16 plot(z1, w1, 'r*');
17 F1 = @(x1, z1) x1(1)*sqrt(1+(((z1-x1(2)).^2)*2.4025/(100000000*(pi
    ^2)*(x1(1))^4)));
18 x10 = [0.05 0];
19 [x1, resnorm, ~, exitflag, output] = lsqcurvefit(F1, x10, z1, w1);
20 b1 = (-300:0.01:120);
21 a1 = x1(1)*sqrt(1+(((b1-x1(2)).^2)*2.4025/(100000000*(pi^2)*(x1(1)
    ^4)));
22 plot(b1, a1, 'r');
23
24 plot(z2, w2, 'b*');
25 F2 = @(x2, z2) x2(1)*sqrt(1+(((z2-x2(2)).^2)*2.4025/(100000000*(pi
    ^2)*(x2(1))^4)));
26 x20 = [0.05 0];
27 [x2, resnorm, ~, exitflag, output] = lsqcurvefit(F2, x20, z2, w2);
28 b2 = (-300:0.01:120);
29 a2 = x2(1)*sqrt(1+(((b2-x2(2)).^2)*2.4025/(100000000*(pi^2)*(x2(1)
    ^4)));
30 plot(b2, a2, 'b');
31
32 k1 = min(a1);
33 k2 = min(a2);
34
35 title('Beam Profile');
36 xlabel('Distance (cm)');
37 ylabel('Beam Width (cm)');
38 legend('Collimator', 'Vertical', 'Collimator', 'Horizontal');
39 hold off;

```